Numerical models of the inversion of half-graben basins

Susanne J. H. Buiter[1] and O. Adrian Pfiffner

Institute of Geological Sciences, University of Bern, Bern, Switzerland

[1] We investigate the dynamic evolution of fold and thrust structures which form by compression and inversion of a sequence of half-graben basins. The choice for a half-graben geometry is motivated by seismic studies and reconstructions of preinversion geometry of inverted regions, which show that rifting often leads to a series of half-grabens. To examine the deformational structures which result from basin inversion, we use a two-dimensional, viscous-plastic numerical model and start our experiments from a preexisting extensional geometry. We find that synrift and postrift sediments are uplifted in the initial stages of basin inversion. This uplift is accompanied by rotation of the basement blocks beneath the basins. In the postrift sequence new shear zones form which are a continuation of basin-bounding faults. With continuing shortening, further inversion is more difficult owing to relative strengthening of the half-graben region. Significant surface erosion facilitates inversion. Back thrusts mainly develop in association with listric basin-bounding faults and less for planar (domino array) faults. Weak sediments (such as salt or shales) at the base of the basins promote the development of basement shortcut faults. The presence of a postrift decollement layer tends to decouple deformation of the postrift sediments from the material below it. In our model, preexisting weak basin-bounding shear zones are a requirement for substantial amounts of basin inversion to occur. Our numerical model results display many first order characteristics of examples from nature and analogue studies. *INDEX TERMS:* 8020 Structural Geology: Mechanics; 3210 Mathematical Geophysics: Modeling; 8105 Tectonophysics: Continental margins and sedimentary basins (1212); 8110 Tectonophysics: Continental tectonics—general (0905); *KEYWORDS:* basin inversion, half-graben, finite element method. **Citation:** Buiter, S. J. H., and O. A. Pfiffner, Numerical models of the inversion of half-graben basins, *Tectonics*, *22*(5), 1057, doi:10.1029/2002TC001417, 2003.

---

[1]Now at Geodynamics Group, Department of Oceanography, Dalhousie University, Halifax, Nova Scotia, Canada.

1. Introduction

[2] The evolution of sedimentary basins is governed by their surrounding stress field and can, therefore, be expected to be highly sensitive to variations in these stresses. In this paper we are concerned with regions where extension and/or rifting occurred and which underwent compression in later stages of their evolution. In the North Sea region, for example, extension was in the Late Cretaceous replaced by compression, probably related to the Alpine collision [*Ziegler et al.*, 1995]. The Alpine mountains themselves were built on a passive margin structure [*Lemoine and Trümpy*, 1987; *Schmid et al.*, 1996]. It is to be expected that sedimentary basins which were formed during the extensional phase are inverted when the stress field is reversed. By basin inversion is meant here the evolution of a basin which is formed by extension and has later undergone compression whereby the basin fill is uplifted and partially extruded, and preexisting faults are reused [*Cooper et al.*, 1989]. Mild to moderate basin inversion has been identified, for example, on seismic profiles in the North Sea and the Alpine foreland [*Ziegler*, 1983; *Badley et al.*, 1989]. It is characterized by uplift of the basin fill, folding of synrift and postrift sediments and (partial) reactivation of normal faults. Examples of strong or complete inversion can be found in the Alps and Pyrenees [*Bally*, 1984; *Gillcrist et al.*, 1987; *de Graciansky et al.*, 1989]. Folding, faulting, fault rotation, fault reactivation and extrusion of the basin fill play a role in the generation of sometimes complex deformational structures.

[3] Field observations and seismic studies have found various factors which are expected to control the structural style of basin inversion [*Ziegler*, 1983; *Gillcrist et al.*, 1987; *Hayward and Graham*, 1989; *Coward et al.*, 1991]. These include: the capability of faults for reactivation [see also *Sibson*, 1985; *Etheridge*, 1986], whether faults are planar or listric, the buttressing effect of normal faults, the preinversion geometry of the basin, the amount of shortening, lithospheric strengthening after rifting, and lithology. With numerical and analogue models it is possible to systematically investigate the effects of (variations in) these factors on structures developing during basin inversion. Results may be used to identify the factors that are relevant to basin inversion, provide help in the interpretation of seismic and field data, and provide criteria for recognizing basin inversion.

[4] Most previous model studies of basin inversion used analogue modeling techniques. *Nalpas et al.* [1995] [see also *Brun and Nalpas*, 1996] show how the presence of a decollement layer (model equivalent of Zechstein salt in the North Sea) decouples the cover from the basement and

enhances the development of low angle thrust faults above the graben boundary faults. Reactivation of extensional normal faults occurs for oblique compression (i.e., when the angle between compression and the graben axis is smaller than 45°). The influence of footwall geometry was investigated by *Buchanan and McClay* [1991] in experiments of an inverted listric or planar fault. The hanging wall structures which develop for both cases are, surprisingly, rather similar. During inversion the detachment fault is reactivated and propagates steeply upward into the postrift sequence. The tips of intra-basinal extensional faults serve as nucleation points for the creation of new reverse faults. A limitation to these experiments is the fact that the footwall to the fault is rigid. Shortcut faults through the footwall are, therefore, impeded. *Buchanan and McClay* [1992] examine basin inversion above an array of domino faults. In their set-up, fault-bounded basement blocks are rigid, but are allowed to rotate. Contraction leads to reactivation of the domino faults, their propagation into the postrift sequence and the development of footwall shortcut faults in the sediments. Footwall folding occurs only in case of an anisotropic material sequence in which interlayer slip is facilitated.

[5] In our study of basin inversion structures, we use a two-dimensional numerical model. Advantages of a numerical method over an analogue method are, for example, the possibility of tracking of stresses and strains during the evolution of the model, the relatively large freedom in choice of material properties and boundary conditions, and a relatively easy implementation of temperature-dependent rheologies. Due to its two-dimensional character, we cannot use our model to investigate, for example, extension followed by transpression. Few previous studies exist (at least that we are aware of) of numerical simulations of basin inversion. *Nielsen and Hansen* [2000] [see also *Hansen et al.*, 2000] investigate the consequences of the presence of a crustal weak zone during compression using an elastovisco-plastic thermomechanical model which includes sedimentation and erosion. Their results show an uplifting inversion zone flanked by marginal troughs, which result from flexure of the relatively strong upper mantle.

[6] We examine the effects of compression of a sequence of half-graben basins. Our choice for a half-graben geometry is motivated by seismic studies, which show that rifting often leads to a series of half-grabens [e.g., *De Charpal et al.*, 1978; *Cheadle et al.*, 1987], and by reconstructions of preinversion geometry of inverted regions [*Lemoine and Trümphy*, 1987; *Gillcrist et al.*, 1987; *de Graciansky et al.*, 1989]. Already reflected in the description of basin inversion [*Cooper et al.*, 1989] is the importance of the reactivation of extensional faults. Since we are not interested in the conditions for fault reactivation, but instead in structures resulting from the inversion of a basin, we examine basins bounded by preexisting weak faults. Faults can be weak relative to their surroundings due to high pore-fluid pressures or strain softening processes.

[7] The aim of our study is to investigate the effect of various factors which play a role in the development of deformational (folds and thrusts) structures forming during the inversion of half-grabens. We focus on the sensitivity of
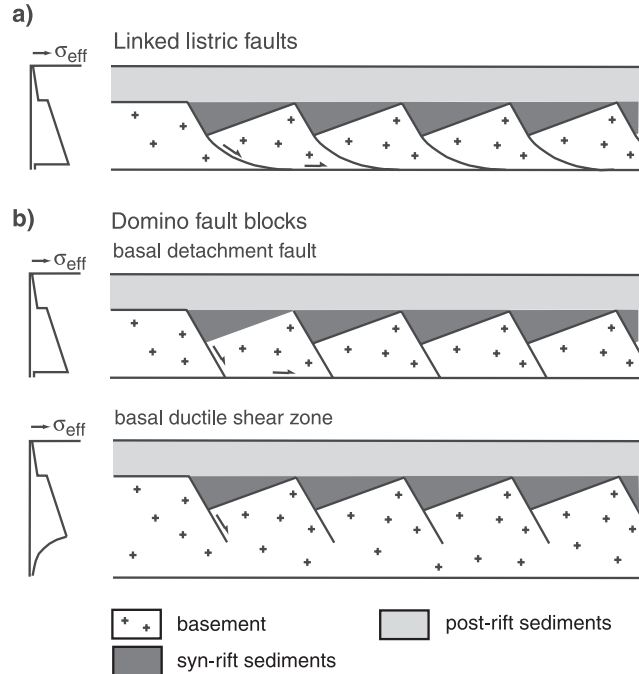

Figure 1. Illustration of possible geometries of the fault-bounded blocks below half-graben basins. (a) Linked listric faults. The basin-bounding faults merge in a common basal detachment fault. (b) Domino fault block model. The basin-bounding faults end in a basal detachment (top) or the displacement along the faults is taken up by ductile deformation deeper down (bottom). The stress profiles are schematic representations of the initial effective stress on the left-hand side of the models. The small arrows indicate the sense of movement along the faults during extension.

evolving structures to inherited extensional geometry (listric or planar faults), synrift and postrift competence contrast, the presence of weak decollement layers, and surface erosion. Results of our models are compared with examples from nature (seismic and field studies) and analogue studies.

2. Fault Block Geometries

[8] Half-graben basins are generally bounded on one side by a normal fault which dips around 60° or less (possibly due to later rotation) and continues to depths below the basin. As the basin grows during extension, materials of varying strengths (e.g., shales, sand, carbonates) may be deposited accumulating a sedimentary fill which can be on the order of some kilometers thick [e.g., *De Charpal et al.*, 1978]. After extension, subsidence due to thermal reequilibriation will facilitate the deposition of postrift sediments.

[9] Two geometries are generally considered for the fault-bounded blocks below the half-graben basins: linked listric fault [*Wernicke and Burchfiel*, 1982; *Gibbs*, 1984] or domino fault blocks [*Mandl*, 1987; *Davison*, 1989]. In the linked listric faults model (Figure 1a), listric basin-bounding faults merge in a common basal detachment. The fault-
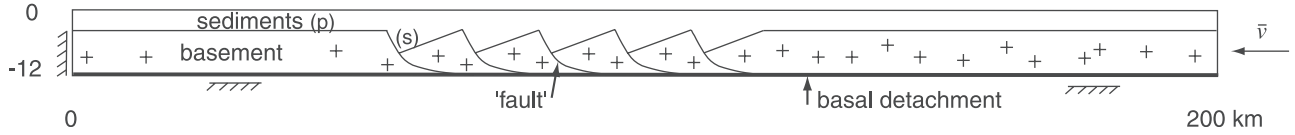
Figure 2. Initial geometry and boundary conditions for the linked listric fault model. The geometry represents the end of an extension phase which created a sequence of half-graben basins. The basins and the basement next to them are covered by a layer of postrift sediments (p). The basins are filled with synrift sediments (s). The basin-bounding "faults" merge in a common basal detachment. The model is compressed through a velocity $\bar{v}$ at the right-hand side. The basement at the left-hand side is held fixed. The postrift sediments above it are allowed to flow out horizontally. No thickening or thinning occurs at the side boundaries. The base of the model is held fixed. Diffusive erosion is imposed at the surface.

bounded blocks rotate during extension, but the faults themselves need not necessarily be rotated. Sedimentary layers typically show a differential tilt across a basin-bounding listric fault. Faults in the domino model (Figure 1b) are planar and (almost) parallel. Extension is achieved by simultaneous rotation of all blocks. Fault dip, therefore, decreases with increasing amount of extension. The transition from the rotating blocks to the unstretched sides can be accommodated by deformation of the rift margins and external fault blocks or by the presence of a listric-fault [*Wernicke and Burchfiel*, 1982; *Davison*, 1989].

[10] In the case of the domino fault model an assumption has to be made regarding the deformation style and continuation of the faults below the basins. We consider two cases (Figure 1b). In the first the domino faults end in a basal detachment fault. This setup is inspired by the analogue models of *Buchanan and McClay* [1992] of extension and subsequent inversion above domino faults. In their experimental setup rigid fault blocks are simulated by a set of parallel plates which are connected to a horizontal base along which uniform displacement takes place. In the second case we assume that the brittle deformation along faults is taken over by ductile deformation at deeper levels. In this setting a basal detachment fault is not required.

3. Modeling Method

[11] We use a two-dimensional numerical model to study the deformational structures which result when a half-graben sequence, as described above, is compressed. By limiting the model to the upper crust, we achieve a high resolution. The depth of the model domain is determined by either the depth to a basal detachment or the depth at which the ductile strength is low. The general aspects of our initial geometry are illustrated by the starting geometry for the linked listric faults model (Figure 2). It consists of five half-grabens which are each 4 km deep. The basin-bounding faults dip 60°, while the other side of each basin dips 20°. The postrift sequence is 4 km thick. The complete model extends to 12 km depth. When ductile deformation at depth is included, the model is 16 km deep.

[12] We solve the equations of mechanical equilibrium for incompressible flows using the finite element code "Sopale," developed by P. Fullsack [*Fullsack*, 1995; see also *Willett*, 1999]. The code uses the arbitrary Lagrangian-Eulerian formulation. All calculations are performed on an Eulerian grid to which material properties are assigned

using separate Lagrangian material tracking points. After each time step, the Eulerian grid is allowed to thicken or thin vertically based on the Eulerian displacements and surface processes of that time step. The plane strain approximation is adopted. For a model domain of 200 × 12 km we use 24,000 rectangular elements and 123,369 material tracking points. This mesh resolution leads to a thickness for the basin-bounding faults and the basal detachment of around 600 m (based on a minimum of 3 Eulerian elements in each of these layers). Calculations with a higher element and material tracking point density confirm that the models have converged.

[13] The model materials deform according to a viscous-plastic rheology (Table 1). At the upper crustal depths considered in our study most materials (i.e., basement, basin fill and postrift sequence) show frictional-plastic behaviour. We adopt a Coulomb yield criterion: $\sigma_E = C - p\, sin\phi$, where σ_E denotes effective stress, C cohesion, p dynamic pressure and ϕ the internal angle of friction. The dynamic pressure contains a gravitational (lithostatic) component and a component due to the applied boundary conditions. Model deformation is continuous and faults are not discrete planes, but shear zones along which large deformation can be accommodated. These shear zones form in a dynamic manner in response to the model evolution and they are typically initiated by (material) inhomogeneities. All shear zones initially develop at an angle of 45° to the direction of maximum compression, both in compression and in extension. However, they usually do not retain this 45° dip, since they flatten or steepen during further model evolution as determined by local deformation and rotation. Materials representing evaporites or shales are assigned a weak linear (Newtonian) viscous rheology. We assume that preexisting normal faults are weaker than the surrounding material, due to, for example, high pore fluid pressures or strain softening. Preexisting extensional faults are simulated by a zone of weak linear viscous material [e.g., *Boutilier and Keen*, 1994]. The basal detachment fault which is present in most of the models is simulated by a weak linear viscous layer as well. The viscosity of the Newtonian materials was chosen such that it is weak in comparison with the other materials (model sediments and basement), but strong enough to remain numerically stable. In one category of the domino fault block models, ductile deformation at depth is important. We use a weak power-law flow law (for wet quartzite of *Jaoul et al.* [1984]) to bring its effects out clearly and to limit the depth extent of the model. The temperature

Table 1. List of Models[a]

Model	Fault Geom.	Rheol.[b]	Surf. Proc.[c]	Synrift Sed.[d]	Postrift Sed.[d]	Basal Detach.[e]	Figure
L1	listric	frp	diff.	15°/10	15°/10	lv 10^{20}	3
L2	listric	frp	none	15°/10	15°/10	lv 10^{20}	4
L3	listric	frp	total	15°/10	15°/10	lv 10^{20}	4
L4	listric	frp	diff.	30°/30	30°/30	lv 10^{20}	5
L5	listric	frp	diff.	20°/15	10°/5	lv 10^{20}	5
L6	listric	frp	diff.	10°/5	20°/15	lv 10^{20}	5
L7	listric	frp	diff.	lv 10^{20} & 15°/10	15°/10	lv 10^{20}	6
L8	listric	frp	diff.	15°/10	lv 10^{20} & 15°/10	lv 10^{20}	6
L9	list, 10^{21}	frp	diff.	15°/10	15°/10	lv 10^{20}	7
L10	list, 5×10^{21}	frp	diff.	15°/10	15°/10	lv 10^{20}	7
L11	listric	frp	diff.	15°/10	15°/10	frp 4°	–
L12	listric	frp	diff.	15°/10	15°/10	frp 8°	–
D1	domino	frp	diff.	15°/10	15°/10	lv 10^{20}	8
D2	domino	vp	diff.	15°/10	15°/10	none	8

[a]For all models the basement has an angle of internal friction of 30°, a cohesion of 30 MPa and a density of 2800 kg m^{-3}. All sediments have a density of 2600 kg m^{-3}.

[b]Abbreviations are as follows: frp, frictional-plastic; vp, viscous-plastic.

[c]Surface processes: diffusive erosion, no surface processes, or total erosion.

[d]Angle of internal friction/Cohesion (MPa); lv, linear viscous (viscosity in Pa s).

[e]Abbreviations are as follows: lv, linear viscous (viscosity in Pa s); frp, frictional-plastic (with angle of internal friction).

evolution is in this case determined by a surface heat flow of 60 mW m^{-2}, a heat production of 1 μW m^{-3}, and a thermal diffusivity of 10^{-6} m^2 s^{-1}. This results in a low strength at 16 km depth. Therefore, this depth is adopted for the base of this model. The transition between frictional-plastic and ductile behaviour is determined dynamically by the model and is not imposed a priori. For a strain rate of 10^{-15} s^{-1} the transition initially lies at 8.3 km depth.

[14] Compression is achieved by pushing the right-hand side of the model with a velocity of 1 cm/yr (Figure 2), until a total displacement in the range of 10 to 50 km is reached. The basement on the left-hand side of the model is held fixed. The cover above the basement is allowed to flow out horizontally. We have verified that this outflow condition does not affect the evolving basin inversion structures by comparing results with those for a longer model in which all of the left-hand side was held fixed. The base of the model is fixed. The surface is either free or surface processes may be imposed. We have modified the code to include diffusive erosion [*Culling*, 1960].

[15] Our model is designed to simulate the main features of basin inversion. However, precisely because it is a model, it can not capture all aspects of the often complex deformation occurring in the real Earth. We consider the main limitations to our modeling approach to be: (1) Our models are two-dimensional. Extension followed by oblique convergence [*Brun and Nalpas*, 1996] cannot, therefore, be examined. (2) The rheology of the model materials is viscous-plastic, without elasticity. This means that our model stresses are probably lower than for the case in which elastic behaviour would be part of the model rheology. (3) Flexural compensation of changes in mass is not taken into account. Since we are interested in upper crustal structures developing above a (semi-)horizontal detachment fault, we expect that the effect of this assumption will be small. (4) All shear zones initially develop with a dip of 45°. We do not reproduce dip angles which are commonly

expected for upper crustal materials (where thrust faults initially dip 30° and normal faults 60°, approximately).

4. Inversion of Listric Fault Half-Grabens

4.1. Reference Model

[16] The first model shown here (model L1 in Table 1) is designed to be relatively uncomplicated, while still capturing the main deformational features. It serves as a reference against which the other models are compared. The half-grabens are bounded by preexisting, weak, listric fault zones which merge in a common basal detachment (Figure 3a). The synrift and postrift sediments have the same rheological properties and are both weaker than the basement. No prerift sediments are present. At the surface diffusive erosion acts with a diffusion coefficient of 10^{-6} m^2 s^{-1}.

[17] Figures 3b–3d show the evolution of the reference model at three stages during shortening, from mild inversion (after 0.5 Myr) to strong inversion (after 3 Myr). The figure is centered on the basin sequence. At the right-hand side boundary of the model (outside of Figure 3), thrusts develop which take up part of the shortening which is imposed at that side. These thrusts do, however, not reach the basins in the time span studied here. Shortening results in inversion of the half-grabens. The synrift sediments are uplifted above the level they occupied before compression started. The basement blocks below the basins rotate clockwise upward, this motion is accommodated along the preexisting weak faults.

[18] Deformation is mostly localized in the preexisting weak zones. Corresponding antithetic shear zones develop as well, deforming the synrift sediments. Deformation does not propagate beyond the left-most basin. In the postrift sediments new shear zones form which are continuations of the preexisting weak faults. Initially, they have approximately the same dip angle as the preexisting faults (60°), but with time their dip angle decreases to around 45° to 50°.
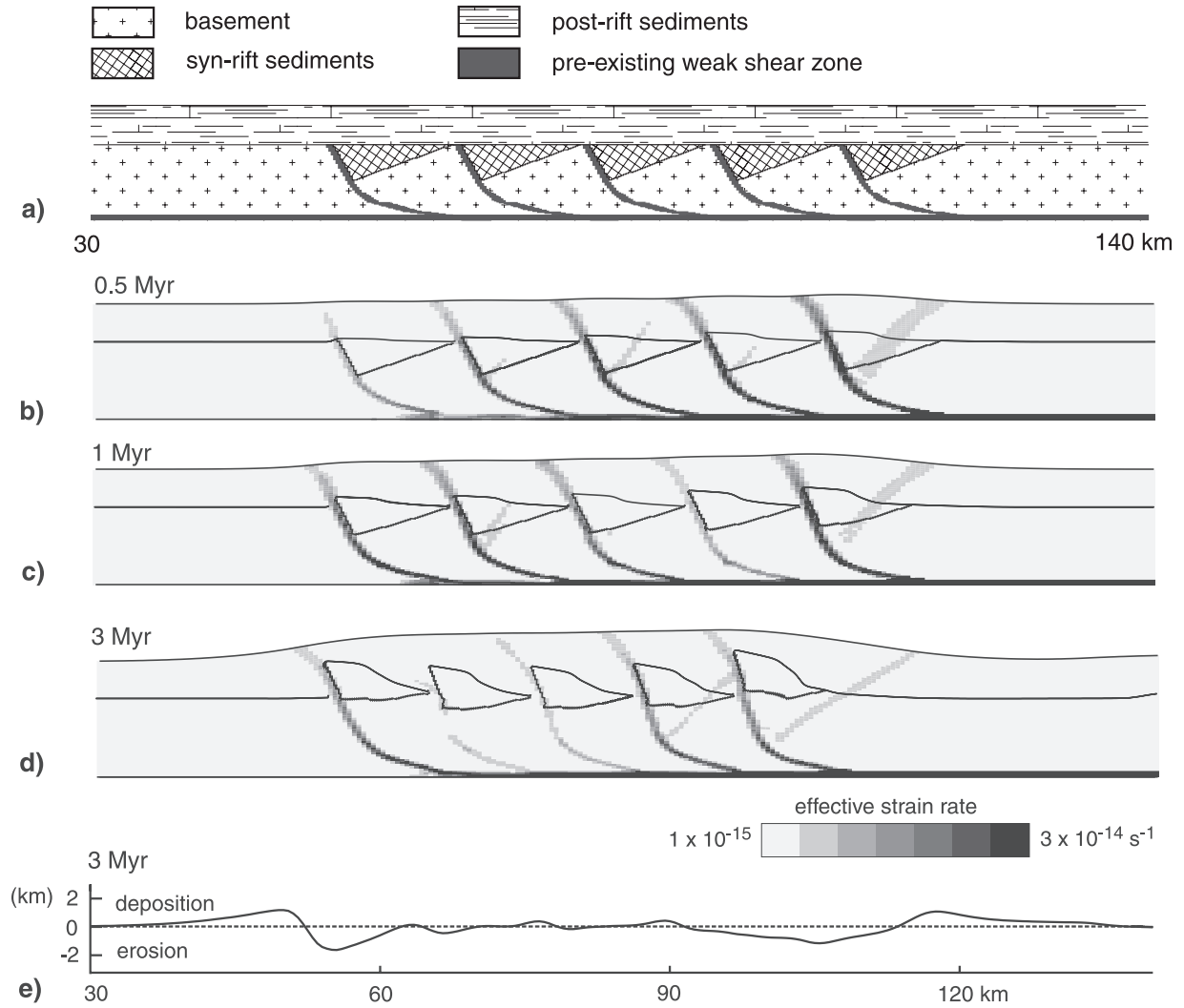
Figure 3. Inversion of half-graben basins (reference model L1). (a) Initial geometry and materials. The material properties are given in Table 1. (b) Geometry and effective strain rate for mild inversion after 0.5 Myr of shortening with 1 cm/yr (5 km shortening). The synrift sediments are uplifted. The shear zones in the postrift sequence are continuations of the preexisting basin-bounding faults. Also weaker antithetic shear zones form. (c) Inversion after 1 Myr (10 km shortening). (d) Strong inversion after 3 Myr (30 km shortening). Note that the basement below the basins has now been uplifted to the level of the basement next to the basin sequence. (e) Total amount of eroded and deposited material after 3 Myr. The diffusion coefficient is 10^{-6} m^2 s^{-1}. The figures are centered on the half-grabens. The whole model is 200 km wide.

The basin-bounding faults steepen with increased shortening (with around 10° after 3 Myr).

[19] With time, the inversion of the basins propagates slightly from right (where the velocity is applied) to left (Figures 3b–3d). We explain this behaviour as a consequence of the interaction between the weak normal faults and the overlying frictional-plastic postrift layer. The latter has a stress gradient from right to left, which causes a lateral variation in the conditions at the intersection points between the faults and this layer. An equivalent model result is obtained in case the basal detachment is weak frictional (with an angle of internal friction of 4°, model L11). An increase in strength of such a frictional basal detachment brings the propagation effect out more clearly. For example, for an increase in the angle of internal friction with a factor of two (i.e., to 8°, model L12) the right-most basin shows approximately the same degree of inversion after 3 Myr as in the reference model, while the left-most basin is not inverted at all.

[20] After 3 Myr of shortening the top of the basement below the half-grabens has been uplifted to the same level as the basement next to the basins (Figure 3d). Since the

sediment pile above the half-grabens is higher than in the neighboring regions, and the yield strength is pressure-dependent, the half-grabens are at this stage relatively strong compared with locations within the rest of the model. Further inversion is, therefore, difficult. This can also be seen from the low strain rates in the half-grabens region. Deformation is transferred to the right-hand side boundary of the model.

[21] Diffusive erosion maximizes erosion and deposition in areas with a large surface curvature. In our model, this is at both ends of the half-graben sequence (Figure 3e). The maximum amount of eroded material in 3 Myr is 1.6 km; therefore, the surface erosion rate is 0.5 mm/yr at maximum.

4.2. Effect of Erosion and Sedimentation

[22] Diffusive erosion redistributes material at the surface. The amount of eroded or deposited material is determined by the diffusion coefficient and the surface curvature. For the reference model, we have chosen the diffusion coefficient such that the maximum surface erosion rate is between 0.4 and 0.6 mm/yr. For comparison, average surface erosion rates for the Alpine mountains are around 0.2–0.4 mm/yr [*Schlunegger and Willett*, 1999; *Kuhlemann et al.*, 2001].

[23] Previous studies have shown that surface processes have an effect on the development of internal deformational structures [*Beaumont et al.*, 2000; *Willett et al.*, 1993]. We examined the influence of the erosional and depositional processes by calculating two end-member models: (1) no surface processes (model L2 in Table 1) and (2) total surface erosion (model L3) (Figure 4). The difference after 10 km of shortening between the reference model (Figure 4b) and the case without erosion (Figure 4a) is very small. In the case where all material uplifted above the initial upper surface is eroded (Figure 4c), the inversion of the half-grabens is facilitated. As long as the basins represent a relatively weak part of the model, deformation concentrates there and inversion continues. During inversion, however, the region of the basins becomes stronger. This strengthening is caused by the overall thickening in this area in combination with the fact that the yield strength is pressure-dependent. Also, most effective thickening takes places in the basement (through block rotation) which is stronger than the sediments above. Total erosion reduces the amount of sediments, and thus the overall thickening, making the basins area in the total erosion case weaker than in the situation with diffusive erosion or no erosion. Therefore, inversion is in this case faster.

4.3. Effect of Basin-Fill Material Properties

[24] The rheological properties of the sedimentary sequence in and above the basins may influence the inversion of the half-grabens. For example, deformation would normally proceed more easily in weaker material. We have, therefore, examined different combinations of material properties of the synrift and postrift sediments (Figure 5, models L4, L5 and L6). Our experiments show differences in deformation of the basin fill and in the principal stresses. Higher stress values can be maintained for stronger materials (higher internal angle of friction and/or cohesion), suppressing deformation of strong synrift sediments (Figure 5b). The basin fill is more deformed for the case where the synrift sediments are weak (Figure 5d). The evolution of the model is for a large part determined by the preexisting weak faults, as can be seen from the case where all material properties are equal (except for the fault zones) (Figure 5b). The compressive stresses in the basin fill are not all horizontal due to internal shear and the close presence of the weak basin-bounding faults. The latter also causes the rotation of the stress field in the lower part of the basement blocks.

4.4. Effect of Weak Sediments

[25] At different stages in the evolution of extensional basins weak sediments, like evaporites or shales, could have been deposited in or above the basins. For example, in the first phases of extension, as the Earth's surface starts to subside, shallow seas may form in which evaporites are deposited. Salt deposits in extensional basins can, for example, be found on the Atlantic margin offshore Newfoundland [*Tankard et al.*, 1989] and in the southern North Sea. Inversion of basins in the French Alps occurred in the presence of salt [*de Graciansky et al.*, 1989; *Roure and Colletta*, 1996]. In the Alpine foreland, Permo-Carboniferous basins are covered by postrift, Triassic evaporites, which acted as detachment horizon during Tertiary compression and inversion [*Pfiffner et al.*, 1997]. During inversion, weak sedimentary layers may focus deformation and/or act as decollement layers along which substantial shear can be accommodated. We examined two cases in which basin inversion is influenced by the presence of weak sediments (Figure 6).

[26] The first case represents a situation with weak synrift sediments (model L7, Figure 6a). In the basement blocks shortcut shear zones develop which branch off from the preexisting fault zones and pass through the weak synrift sediments. These shortcut "faults" cause a stronger deformation of the basin fill compared with the reference model (Figure 3). Since part of the compression is taken up by the shortcut faults, the basement blocks show less rotation along the preexisting fault zones.

[27] In the second case, a layer of weak postrift sediments covers the basin sequence (model L8, Figure 6b). The postrift cover above the weak layer is transported over the weak sediments towards the left. After 3 Myr of shortening the offset between cover and basement is 2.5 km on the left-hand side of the model. This amounts to a relative velocity between cover and basement of 0.08 cm/yr on average.

4.5. Effect of Mechanical Properties of Basin-Bounding Faults

[28] In the models shown so far the basin-bounding fault zones were weak. This ensured that the extensional faults were "reactivated" during inversion, in line with the definition of basin inversion [*Cooper et al.*, 1989]. These preexisting weak fault zones determine a large part of the evolution of the models during inversion (Figures 3, 5,
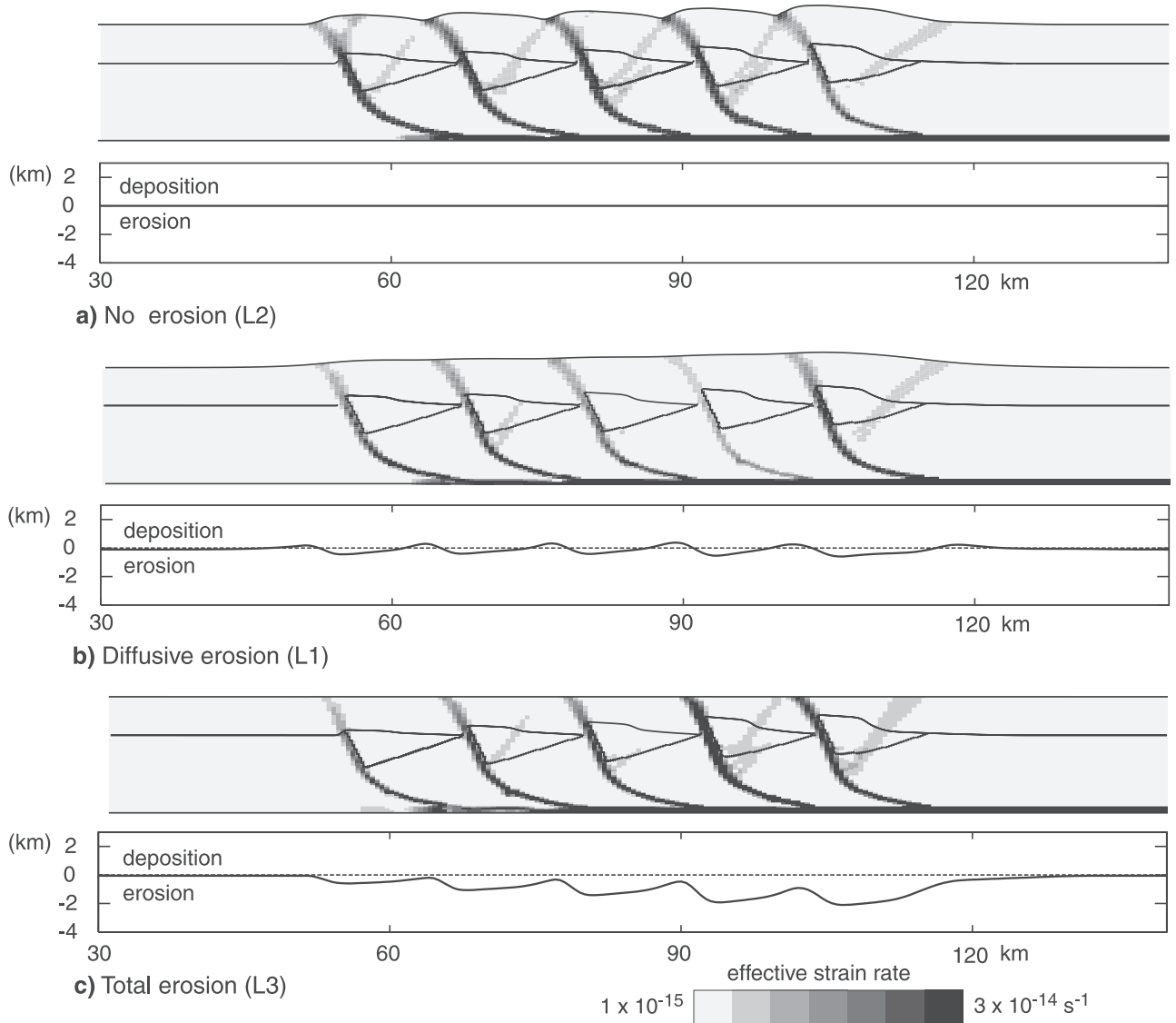
Figure 4. Illustration of the effects of surface processes. (a) No erosion or deposition (model L2). (b) Diffusive erosion with a diffusion coefficient of 10^{-6} m^2 s^{-1} (the reference model L1, Figure 3). Diffusive erosion redistributes material. (c) Total erosion, no sedimentation (model L3). All figures are after 1 Myr of shortening (10 km). Except for the surface processes, the models are identical.

and 6). It is, therefore, relevant to consider what would happen if the preexisting fault zones were stronger. This is illustrated with models L9 and L10 in Figure 7. When the strength of the fault zones is increased (through an increase in viscosity), the inversion proceeds more slowly. More new shear zones develop, deforming the sediments and the basement blocks. The new shear zones branch off from the preexisting fault zones. The latter keep taking up part of the shortening in at least their lowermost part. When the strength of the preexisting faults is 50 times higher than the original value ($\eta = 5 \times 10^{21}$ Pa s, Figure 7c), the uplift of the basin fill due to inversion after 3 Myr of shortening is much reduced. The maximum depth of the basins is still more than 2 km, compared with around zero depth in the

reference model (Figure 6a). In our models, preexisting weak fault zones are, therefore, a requirement for substantial amounts of basin inversion to occur.

5. Inversion of Domino Fault Half-Grabens

[29] Upper crustal extension needs not only lead to the formation of listric basin-bounding faults, but extension can also be accommodated along planar faults (Figure 1). We examined two cases of inversion of domino fault blocks (Figure 8). For both we assume that the basin-bounding fault zones dip with 40° initially, to take into account rotation of the basement blocks during the extensional phase.
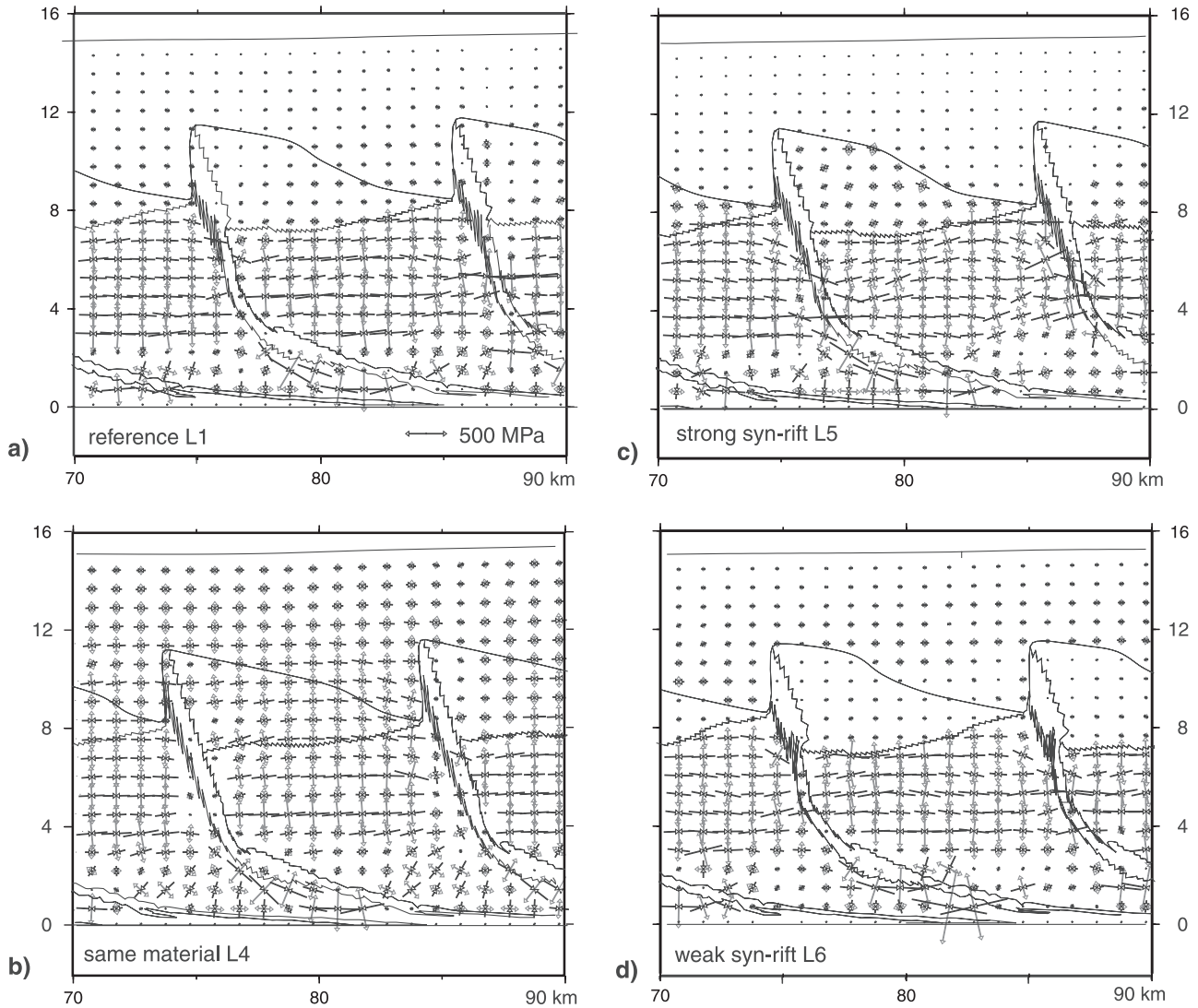
Figure 5. Principal stresses for models with variations in synrift and postrift material properties. The figures are centered on the middle basin and show the results after 3 Myr of shortening. Black arrows denote compression; gray arrows denote extension. The stresses are plotted for every second element in the horizontal direction and every third in the vertical direction. The outlines of the basement blocks, the weak fault zones between the blocks and the synrift sediments are given with thin black lines. (a) Reference model L1 (synrift and postrift sediments have ϕ 15°, C 10 MPa), (b) Model L4, all material properties are equal (ϕ 30°, C 30 MPa), (c) Model L5, strong synrift (ϕ 20°, C 15 MPa) and weak postrift sediments (ϕ 10°, C 5 MPa), (d) Model L6, weak synrift (ϕ 10°, C 5 MPa) and strong postrift sediments (ϕ 20°, C 15 MPa).

[30] In the first case, the planar basin-bounding faults merge in a common basal detachment (Figure 8a, model D1 in Table 1). Deformation during inversion is almost exclusively focused in the preexisting weak fault zones. The basin fills are rotated clockwise and are hardly deformed. The uplift of the basins decreases towards the left (away from the application of the compressional velocity). This propagation effect is more pronounced if the faults dip less steeply. The preexisting fault zones steepen during inversion, whereby the amount of steepening increases toward the right (with around 20° for the right-most fault after 3 Myr).

[31] In the second case, displacement along the planar faults is replaced by ductile deformation at greater depths (Figure 8b, model D2). The base of the model is located at 16 km depth where the ductile strength is very low. Deformation is more distributed in the lower part of the model, owing to the ductile nature of the rheology. The synrift sediments are again rotated clockwise and hardly deformed, except for the right-most basin which is cross
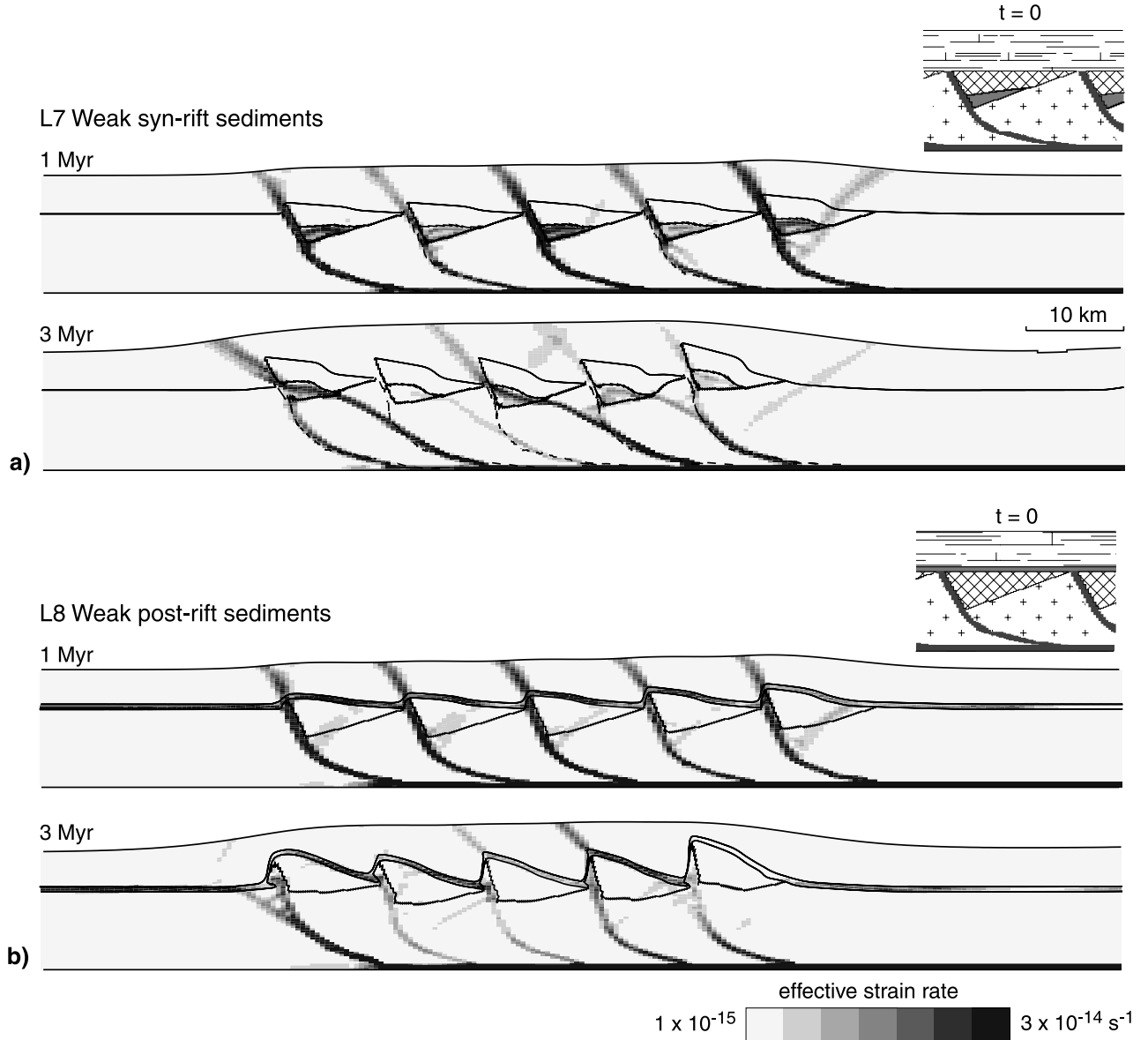
Figure 6. Inversion of the half-grabens is influenced by the presence of a weak layer of sediments (compare with model L1 in Figure 3). (a) Weak synrift sediments (model L7). Note the shortcut shear zones branching off the preexisting faults. The dotted lines are the left sides of the preexisting fault zones. (b) Postrift decollement (model L8). The postrift sediments are transported over the decollement layer toward the left. For both cases the initial position of the weak sediments with respect to the basin is shown in the insets (material coding as in Figure 3). The weak sediments are simulated by a linear viscous material (Table 1). The drawn black lines in the main figures denote the outline of the basin fill and of the weak sediments.

cut by an antithetic shear zone. The basins are uplifted almost simultaneously (except again for the right-most basin).

6. Comparison With Natural Examples

[32] In our numerical simulations of half-graben inversion we find that synrift and postrift sediments in and above the basins are uplifted and rotated during shortening. Since we have prescribed weak basin-bounding faults our setup can not be used to study normal fault reactivation. We find, however, that these faults need to be sufficiently weak in order for basin inversion to take place. In all models new thrust faults form in the postrift sediments which are a continuation of the basin-bounding faults. During shortening the basement below the half-grabens is uplifted and
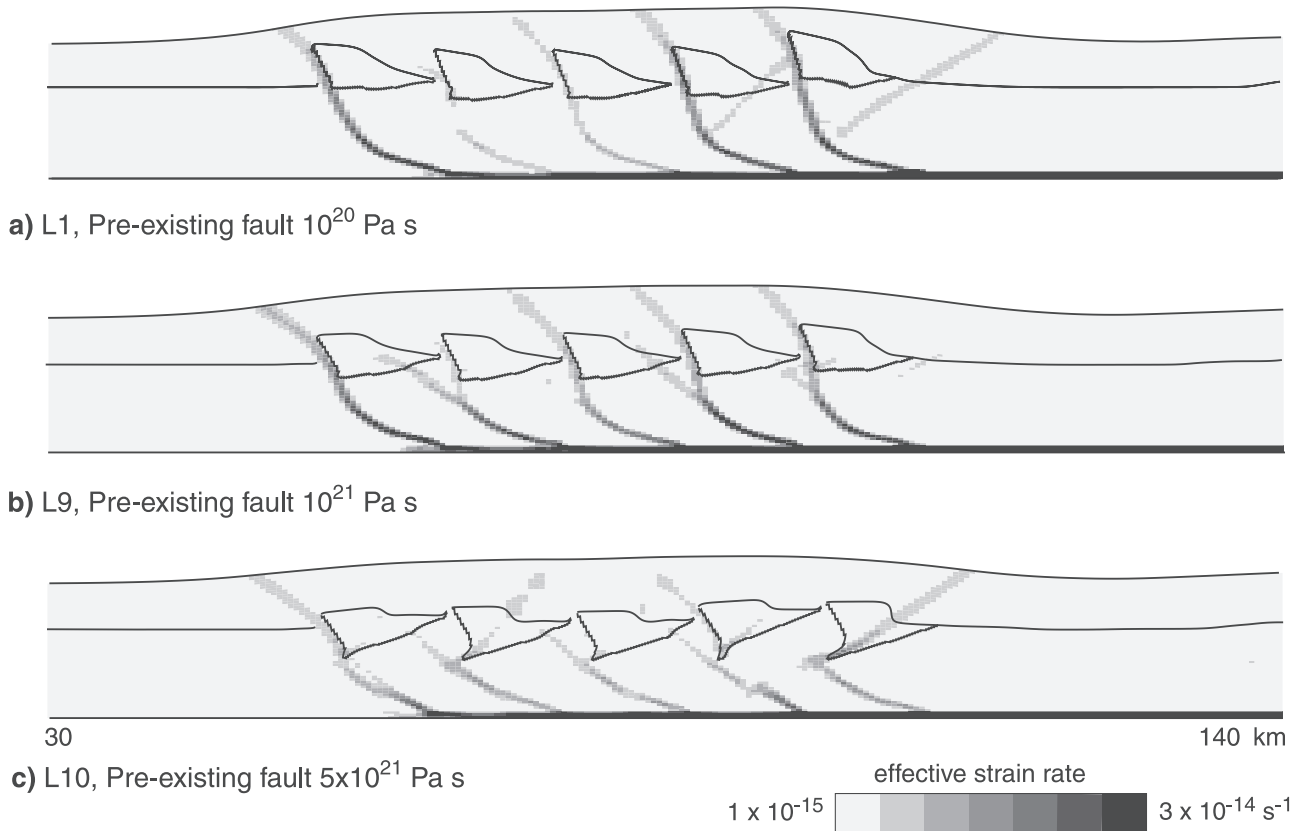
a) L1, Pre-existing fault 10^{20} Pa s

b) L9, Pre-existing fault 10^{21} Pa s

30   140 km

c) L10, Pre-existing fault 5×10^{21} Pa s

effective strain rate

1×10^{-15} 3×10^{-14} s^{-1}

Figure 7. With increasing strength of the preexisting fault zones, inversion of the half-graben basins becomes more difficult. The figures are for fault zone strengths of (a) 10^{20} Pa s (model L1), (b) 10^{21} Pa s (model L9), and (c) 5×10^{21} Pa s (model L10). All figures are after 3 Myr of shortening (30 km).

rotated, until after 25–30 km of shortening (12–15%) the basement is approximately at the same level throughout the model. At this stage the basement has reached its "preextension" level [e.g., *Bally*, 1984]. In our models the basement on either side of the half-grabens does not take up much shortening before this stage. If, however, pure shear thickening would have taken place, the amount of shortening required to bring the basement at one level again would exceed the amount of the preceding extension [*Eisenstadt and Withjack*, 1995]. Back thrusts, and thrusts in the footwall of the basin-bounding normal fault do not form in all cases (compare, for example, Figures 3, 6, and 8).

[33] Many of these general aspects of the evolution of deformational structures in our numerical models agree with examples of half-graben inversion described in literature. In Figure 9 two examples of inversion of half-graben basins are shown. The example from Indonesia [*Letouzey*, 1990] (Figure 9a) shows uplift of synrift and postrift sediments, uplift of the basement below the basin and fault propagation into the sediment cover. These features are also seen in our numerical models. In the example from Germany [*Betz et al.*, 1987] (Figure 9b) the basin-bounding normal fault soles out in a detachment plane in Late Permian (Zechstein) salt. This is similar to our listric fault models (Figures 3 and 6). During inversion the normal fault and its conjugates are

reactivated and the sedimentary sequence in and above the basin is uplifted.

[34] Basin inversion in the presence of potential decollement levels, formed by layers of salt or shales, for example, occurs, among others, in the French Alps and the Alpine foreland. *Roure and Colletta* [1996] describe examples from the French Alps where thrust faults develop in weak sedimentary layers which are present above and in the basin, leading to the development of triangle zones and pop-up structures. In our models weak sedimentary layers also tend to localize deformation during shortening (Figure 6). We only find footwall shortcut "faults" in the case of weak sediments at the base of the synrift sequence.

[35] In the Western Alps *de Graciansky et al.* [1989] and *Gillcrist et al.* [1987] recognized the existence of inverted half-grabens between the Belledonne-Taillefer and the Rochail basement blocks. The situation prior to inversion (Figure 10a) shows a highly asymmetric basin with a master-fault (the Ornon normal fault). The Belledonne-Taillefer basement block acted as rigid buttress upon inversion (Figure 10b). The synrift sequence was intensely folded, developed a penetrative foliation and underwent vertical extrusion in the vicinity of the basement buttress. But inversion also produced back thrusts and asymmetric folds facing in the opposite direction. These back thrusts
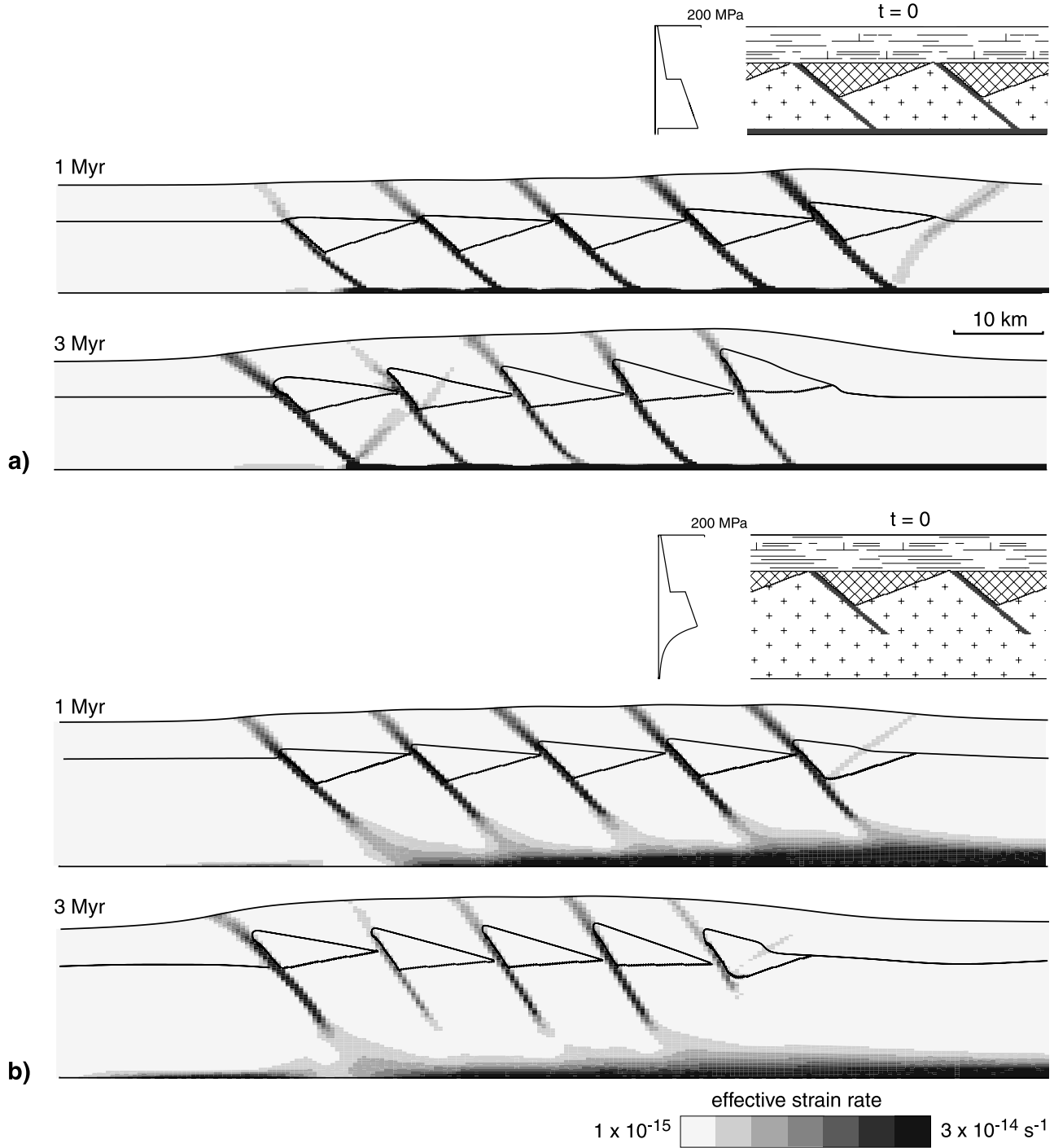
Figure 8. Domino fault block model. The basin-bounding faults dip with 40°, to account for rotation of the fault-bounded blocks during extension. (a) Model D1. The basin-bounding faults merge in a weak basal detachment. (b) Model D2. The basin-bounding faults are replaced by ductile deformation in the lower part of the model. In this case there is no basal detachment fault. Smaller insets show the initial configuration (material coding as in Figure 3) and the initial effective stress profile for the left-hand side of the inset (for Figure 8b) a strain rate of 10^{-14} s^{-1} was used).

a)

b)

base Tertiary

base Upper Cretaceous

base Lias

base Buntsandstein
Zechstein
Carboniferous

base Tertiary

base Upper Cretaceous
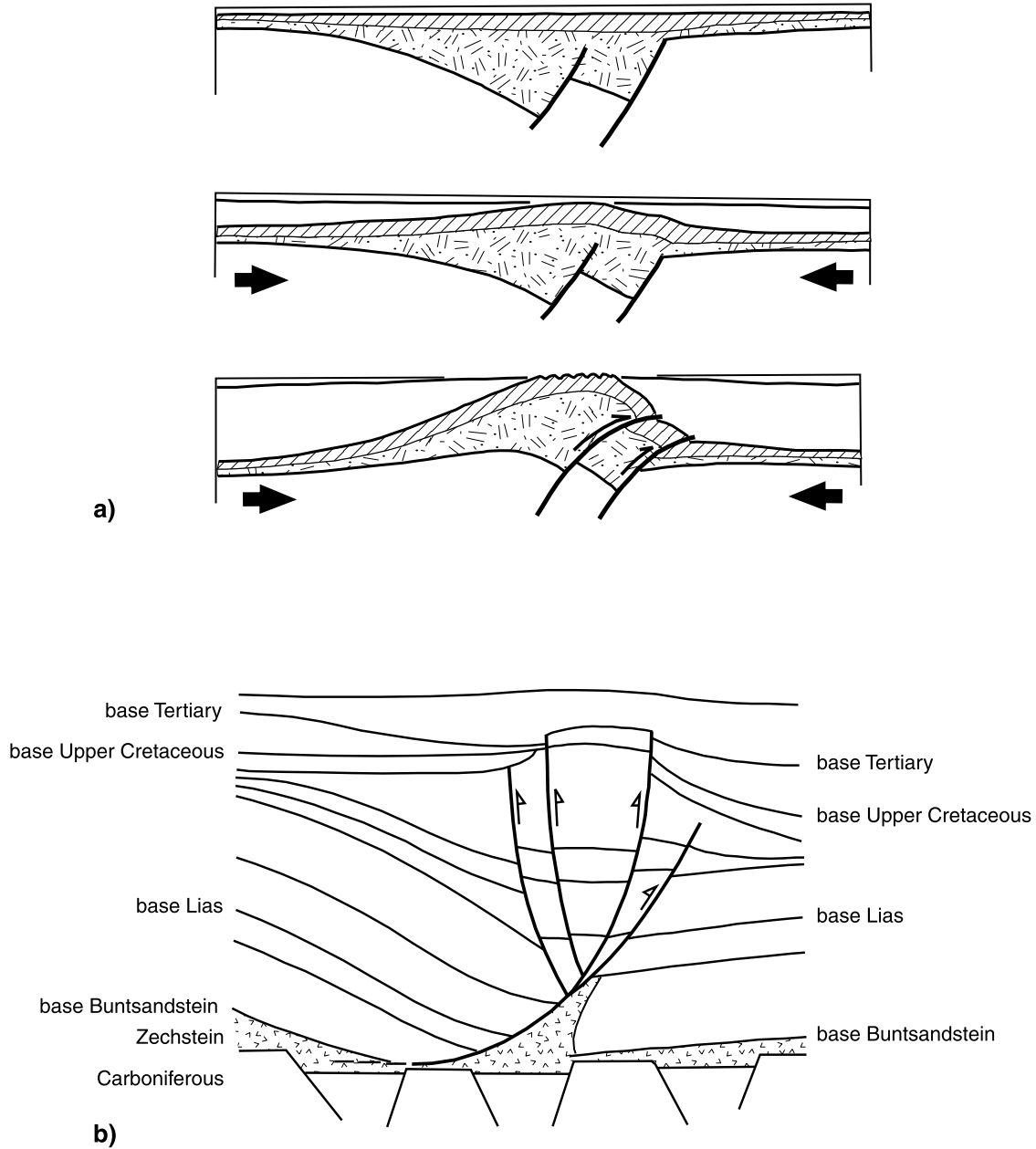
base Lias

base Buntsandstein

Figure 9.   Two natural examples of basin inversion. (a) Scenario of graben inversion on the Eastern Sunda Shelf area in Indonesia [after *Letouzey*, 1990]. (top) Situation at the end of extension and a Middle Miocene tectonic "quiet" period. (middle) Middle Miocene compression. (bottom) Middle to late Miocene inversion with reactivation of the main normal fault. (b) Northern part of the Lower Saxony Basin in Germany. In this region Late Jurassic and Early Cretaceous extension lead to the formation of basins which subsequently became inverted during the Late Cretaceous and Early Tertiary. Figure after *Betz et al.* [1987].

sole into a weak detachment layer near the base of the synrift sequence. Minor normal faults were reactivated as thrust faults, the displacement remaining relatively small. Owing to the large displacement along the Ornon normal fault during extension, subsequent inversion did not bring the graben fill up to the level of the horst. The inversion thereby created a highly asymmetric structure which bears resemblance to the numerical models shown in Figure 6 which include a weak layer at the base of the synrift sequence.

7. Comparison With Analogue Model Studies

[36]   A number of studies have examined the inversion of half-graben basins using analogue modeling techniques. We
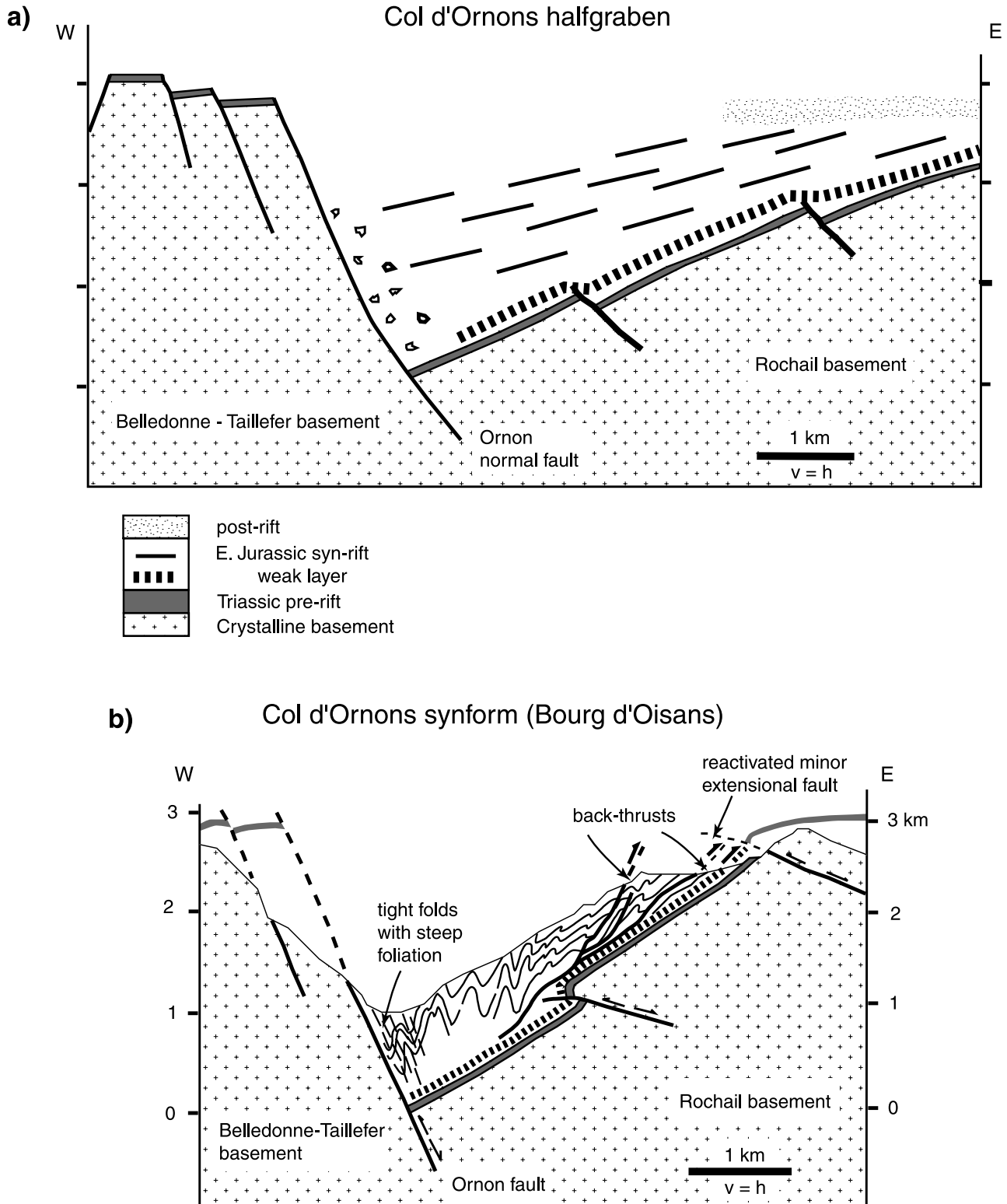
Figure 10. Natural example of basin inversion in the Western Alps. (a) Geometry of the Col d'Ornons half-graben prior to inversion (redrawn after *de Graciansky et al.* [1989] and *Gillcrist et al.* [1987]). (b) Present-day geometry showing tight isoclinal folds in the vicinity of the reactivated Ornon fault, reactivated minor normal faults and back thrusts within the synrift sequence (redrawn after *Gillcrist et al.* [1987] and *de Graciansky et al.* [1989]).
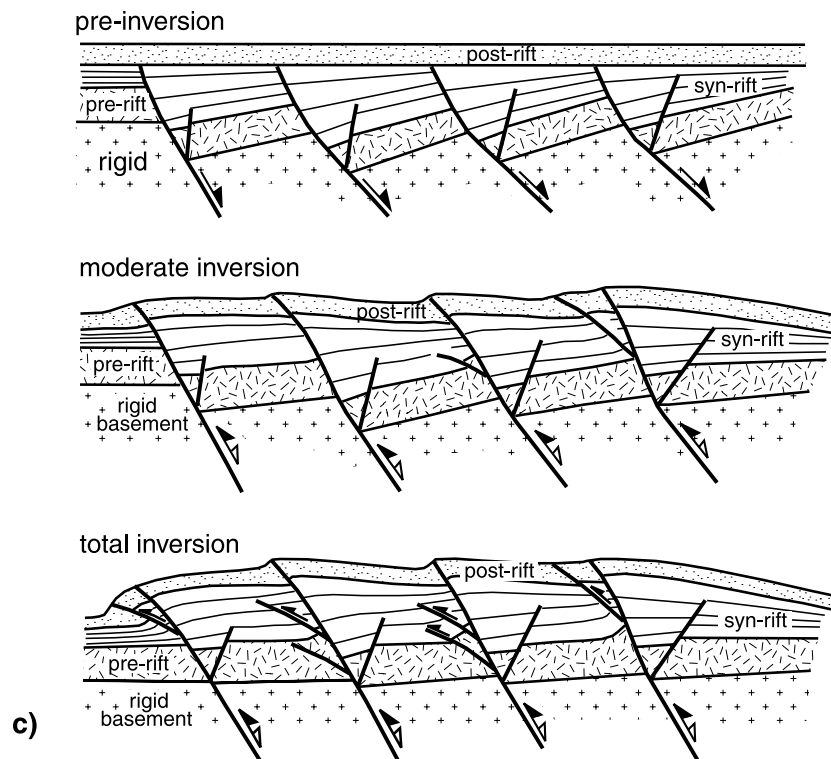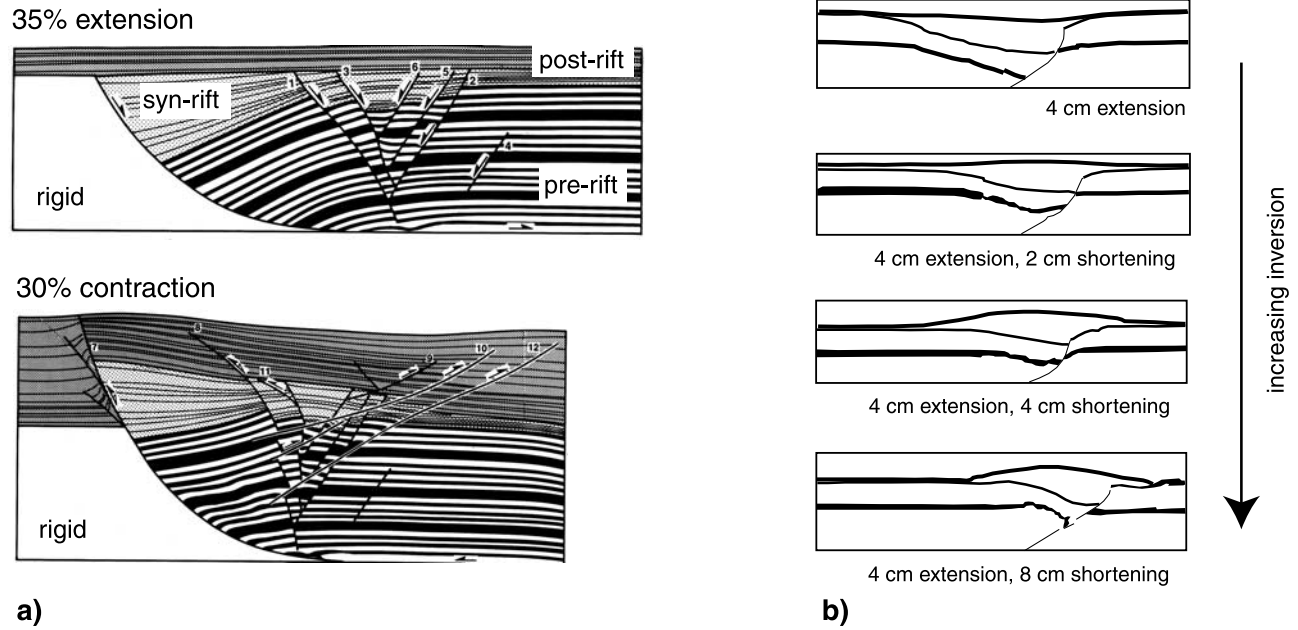
35% extension

30% contraction

a)

4 cm extension

4 cm extension, 2 cm shortening

4 cm extension, 4 cm shortening

4 cm extension, 8 cm shortening

increasing inversion

b)

pre-inversion

moderate inversion

total inversion

c)

Figure 11. Analogue model studies of half-graben inversion. (a) Sandbox study of extension and inversion above a rigid footwall block. The prerift to postrift sedimentary sequence consists of alternate layers of sand and mica [after *Buchanan and McClay*, 1991]. (b) Formation and inversion of a half-graben basin in uniform clay [after *Eisenstadt and Withjack*, 1995]. (c) General line drawing of structures developing in a sandbox during inversion above a domino fault array. The basement blocks (crosses) are rigid [after *Buchanan and McClay*, 1992].

compare our numerical results with three such analogue examples (Figure 11). These examples typically first simulate the formation of the graben and subsequently its inversion. By contrast, we started with a prescribed extensional geometry. In the analogue models described below, the synrift and postrift sediments have the same material properties as the prerift sequence, while in most of our models the synrift and postrift sediments were weaker than the (prerift) basement.

[37] The first example is a sandbox experiment of *Buchanan and McClay* [1991] of extension and inversion above a listric fault (Figure 11a). In their study the footwall to the fault is rigid and deformation of the footwall is, therefore, not possible. The hanging wall (prerift, synrift, and postrift) consists of alternate layers of sand and mica, which makes the sedimentary sequence anisotropic. Even though there are differences in model setup and material properties, our numerical results (Figure 3) show close similarities to the results of this analogue experiment (Figure 11a). During inversion, the basin fill is uplifted and rotated (clockwise in the orientation used here). This is accompanied by upward propagation of the basin-bounding main fault into the postrift sediments. Toward the end of the inversion phase, back thrusts develop in the analogue model. These also develop in our numerical model, but already in an earlier stage. In the results of *Buchanan and McClay* [1991], the first order characteristics of the deformational structures developing during inversion do not change much in case the footwall is planar instead of listric. We find, however, that for planar faults the tendency for back thrusting decreases, resulting in less deformation of the synrift sediments (Figure 8).

[38] The second example is the formation and inversion of a half-graben basin in uniform clay [*Eisenstadt and Withjack*, 1995] (Figure 11b). In this case a main listric normal fault develops above diverging basal plates and the footwall to the fault is deformable. During shortening the main normal fault and secondary normal faults are reactivated as reverse faults, but in most cases not all deformation is recovered. The relative ease with which the normal fault is reactivated justifies a comparison with our results in which preexisting faults are made weak and, therefore, activated in compression. The inversion in the analogue experiments produces an uplift in the synrift and postrift sediments above the half-graben, similar to our models. In the hanging wall and footwall thrust faults develop. We only find footwall thrusts in case weak synrift sediments are present (Figure 6a).

[39] The third example is a study of basin inversion above a domino fault array [*Buchanan and McClay*, 1992] (Figure 11c). Our model of a domino fault array with a basal detachment (Figure 8a) was designed on the basis of this analogue experiment. In the analogue model setup the basement below the prerift sediments consists of rigid blocks, while the basement in the numerical setup is allowed to deform in a brittle manner. In general, our numerical results and the analogue models both show fault propagation into the postrift sediments, and uplift and rotation of the sedimentary sequence. In our model, we do not see the equivalent of sedimentary shortcut faults which develop in the sandbox models.

8. Conclusions

[40] In this study we present results of numerical models that simulate the dynamic evolution of deformational structures developing during compression and inversion of half-graben basins. General features of our models of half-graben inversion are (1) rotation and uplift of sediments in and above the basins, (2) propagation of basin-bounding shear zones upward into the postrift sediments, and (3) restoration of the basement to its (inferred) preextension level. Once the basement has reached a same level throughout the model further inversion is more difficult. Significant surface erosion reduces the amount of sediment overlying the basins and in this manner facilitates inversion. We find that back thrusts develop mainly in association with listric basin-bounding faults and less for planar faults. Weak sediments (model equivalent of shales or salt) localize deformation. Weak sediments at the base of the synrift sequence promote the development of shortcut faults. A weak sedimentary layer at the base of the postrift sediments decouples the cover from the material below it, allowing relative movement of the cover with respect to the basement. In our models, preexisting weak ''fault'' zones are a requirement for substantial amounts of basin inversion to occur. Although our numerical models are simplifications of the natural geologic setting, we are able to simulate some of the primary features of inversion observed in examples from nature and analogue modeling.

References

Badley, M. E., J. D. Price, and L. C. Backshall, Inversion, reactivated faults and related structures: Seismic examples from the southern North Sea, in *Inversion Tectonics*, edited by M. A. Cooper and G. D. Williams, *Geol. Soc. Spec. Publ.*, *44*, 201–217, 1989.

Bally, A. W., Tectogenèse et sismique réflexion, *Bull. Soc. Géol. Fr.*, *26*, 279–285, 1984.

Beaumont, C., H. Kooi, and S. Willett, Coupled tectonic-surface process models with applications to rifted margins and collisional orogens, in *Geomor-*

phology and Global Tectonics, edited by M. A. Summerfield, pp. 29–55, Chichester, New York, 2000.

Betz, D., F. Führer, G. Greiner, and E. Plein, Evolution of the Lower Saxony Basin, *Tectonophysics*, *137*, 127–170, 1987.

Boutilier, R. R., and C. E. Keen, Geodynamic models of fault-controlled extension, *Tectonics*, *13*, 439–454, 1994.

Brun, J. P., and T. Nalpas, Graben inversion in nature and experiments, *Tectonics*, *15*, 677–687, 1996.

Buchanan, P. G., and K. R. McClay, Sandbox experiments of inverted listric and planar faults systems, *Tectonophysics*, *188*, 97–115, 1991.

Buchanan, P. G., and K. R. McClay, Experiments on basin inversion above reactivated domino faults, *Mar. Pet. Geol.*, *9*, 486–500, 1992.

Cheadle, M. J., S. McGeary, M. R. Warner, and D. H. Matthews, Extensional structures on the western UK continental shelf: A review of evidence from deep seismic profiling, in *Continental Extensional Tectonics*, edited by M. P. Coward, J. F. Dewey, and

P. L. Hancock, *Geol. Soc. Spec. Publ.*, *28*, 445–465, 1987.

Cooper, M. A., G. D. Williams, P. C. de Graciansky, R. W. Murphy, T. Needham, D. De Paor, R. Stoneley, S. P. Todd, J. P. Turner, and P. A. Ziegler, Inversion tectonics—A discussion, in *Inversion Tectonics*, edited by M. A. Cooper and G. D. Williams, *Geol. Soc. Spec. Publ.*, *44*, 335–347, 1989.

Coward, M. P., R. Gillcrist, and B. Trudgill, Extensional structures and their tectonic inversion in the Western Alps, in *The Geometry of Normal Faults*, edited by A. M. Roberts, G. Yielding, and B. Freeman, *Geol. Soc. Spec. Publ.*, *56*, 93–112, 1991.

Culling, W. E. H., Analytical theory of erosion, *J. Geol.*, *68*, 336–344, 1960.

Davison, I., Extensional domino fault tectonics: Kinematics and geometrical constraints, *Ann. Tectonicae*, *3*, 12–24, 1989.

De Charpal, O., P. Guennoc, L. Montadert, and D. G. Roberts, Rifting, crustal attenuation and subsidence in the Bay of Biscay, *Nature*, *275*, 706–711, 1978.

de Graciansky, P. C., G. Dardeau, M. Lemoine, and P. Tricart, The inverted margin of the French Alps and foreland basin inversion, in *Inversion Tectonics*, edited by M. A. Cooper and G. D. Williams, *Geol. Soc. Spec. Publ.*, *44*, 87–104, 1989.

Eisenstadt, G., and M. O. Withjack, Estimating inversion: Results from clay models, in *Basin Inversion*, edited by J. G. Buchanan and P. G. Buchanan, *Geol. Soc. Spec. Publ.*, *88*, 119–136, 1995.

Etheridge, M. A., On the reactivation of extensional fault systems, *Philos. Trans. R. Soc. London, Ser. A*, *317*, 179–194, 1986.

Fullsack, P., An arbitrary Lagrangian-Eulerian formulation for creeping flows and its application in tectonic models, *Geophys. J. Int.*, *120*, 1–23, 1995.

Gibbs, A. D., Structural evolution of extensional basin margins, *J. Geol. Soc. London*, *141*, 609–620, 1984.

Gillcrist, R., M. Coward, and J.-L. Mugnier, Structural inversion and its controls: Examples from the Alpine foreland and the French Alps, *Geod. Act.*, *1*, 5–34, 1987.

Hansen, D. L., S. B. Nielsen, and H. Lykke-Andersen, The post-Triassic evolution of the Sorgenfrei-Torn-quist Zone—Results from thermo-mechanical modelling, *Tectonophysics*, *328*, 245–267, 2000.

Hayward, A. B., and R. H. Graham, Some geometrical characteristics of inversion, in *Inversion Tectonics*, edited by M. A. Cooper and G. D. Williams, *Geol. Soc. Spec. Publ.*, *44*, 17–39, 1989.

Jaoul, O., J. Tullis, and A. Kronenberg, The effect of varying water contents on the creep behavior of Heavitree Quartzite, *J. Geophys. Res.*, *89*, 4298–4312, 1984.

Kuhlemann, J., W. Frisch, I. Dunkl, and B. Székely, Quantifying tectonic versus erosive denudation by the sediment budget: The Miocene core complexes of the Alps, *Tectonophysics*, *330*, 1–23, 2001.

Lemoine, M., and R. Trümphy, Pre-oceanic rifting in the Alps, *Tectonophysics*, *133*, 305–320, 1987.

Letouzey, J., Fault reactivation, inversion and fold-thrust belt, in *Petroleum and Tectonics in Mobile Belts*, edited by J. Letouzey, pp. 101–128, Ed. Technip, Paris, 1990.

Mandl, G., Tectonic deformation by rotating parallel faults: The 'bookshelf' mechanism, *Tectonophysics*, *141*, 277–316, 1987.

Nalpas, T., S. Le Douaran, J.-P. Brun, P. Unternehr, and J.-P. Richert, Inversion of the Broad Fourteens Basin (offshore Netherlands), a small-scale investigation, *Sediment. Geol.*, *95*, 237–250, 1995.

Nielsen, S. B., and D. L. Hansen, Physical explanation of the formation and evolution of inversion zones and marginal troughs, *Geology*, *28*, 875–878, 2000.

Pfiffner, O. A., P.-A. Erard, and M. Stäuble, Two cross sections through the Swiss Molasse Basin, in *Deep Structure of the Alps: Results of NRP20*, edited by O. A. Pfiffner et al., pp. 64–72, Birkhäuser Boston, Cambridge, Mass., 1997.

Roure, F., and B. Colletta, Cenozoic inversion structures in the foreland of the Pyrenees and Alps, in *Peri-Tethys Memoir 2: Structure and Prospects of Alpine Basins and Forelands*, edited by P. A. Ziegler and F. Horvath, *Mem. Mus. Nat. Hist. Nat.*, *170*, 173–209, 1996.

Schlunegger, F., and S. Willett, Spatial and temporal variations in exhumation of the central Swiss Alps and implications for exhumation mechanisms, in *Exhumation Processes: Normal Faulting, Ductile Flow and Erosion*, edited by U. Ring et al., *Geol. Soc. Spec. Publ.*, *154*, 157–179, 1999.

Schmid, S. M., O. A. Pfiffner, N. Froitzheim, G. Schönborn, and E. Kissling, Geophysical-geological transect and tectonic evolution of the Swiss-Italian Alps, *Tectonics*, *15*, 1036–1064, 1996.

Sibson, R. H., A note on fault reactivation, *J. Struct. Geol.*, *7*, 751–754, 1985.

Tankard, A. J., H. J. Welsink, and W. A. M. Jenkins, Structural styles and stratigraphy of the Jeanne d'Arc basin, Grand Banks of Newfoundland, in *Extensional Tectonics and Stratigraphy of the North Atlantic Margin*, edited by A. J. Tankard and H. R. Balkwill, *AAPG Mem.*, *46*, 265–282, 1989.

Wernicke, B., and B. C. Burchfiel, Modes of extensional tectonics, *J. Struct. Geol.*, *4*, 105–115, 1982.

Wessel, P., and W. H. F. Smith, New, improved version of the Generic Mapping Tools released, *Eos Trans. AGU*, *79*(47), 579, 1998. [version 3.1]

Willett, S. D., Rheological dependence of extension in wedge models of convergent orogens, *Tectonophysics*, *305*, 419–435, 1999.

Willett, S., C. Beaumont, and Ph. Fullsack, Mechanical model for the tectonics of doubly vergent compressional orogens, *Geology*, *21*, 371–374, 1993.

Ziegler, P. A., Inverted basins in the Alpine foreland, in *Seismic Expression of Structural Styles*, edited by A. W. Bally, *AAPG Stud. Geol.*, *15*, 3. 3/3–3. 3/12, 1983.

Ziegler, P. A., S. Cloetingh, and J. D. van Wees, Dynamics of intra-plate compressional deformation: The Alpine foreland and other examples, *Tectonophysics*, *252*, 7–59, 1995.

———————

S. Buiter, Geodynamics Group, Department of Oceanography, Dalhousie University, Halifax, Nova Scotia, Canada B3H 4J1. (susanne.buiter@dal.ca)

O. A. Pfiffner, Institute of Geological Sciences, University of Bern, Baltzerstrasse 1, CH-3012, Bern, Switzerland. (adrian.pfiffner@geo.unibe.ch)